Unbiased classification of mosquito blood cells by single-cell genomics and high-content imaging

Maiara S. Severo[1], Jonathan J.M. Landry[2], Randall L. Lindquist[3], Christian Goosmann[4], Volker Brinkmann[4], Paul Collier[2], Anja E. Hauser[3,5], Vladimir Benes[2], Johan Henriksson[6], Sarah A. Teichmann[6], Elena A. Levashina[1,7*]

[1]Vector Biology Unit, Max-Planck-Institute for Infection Biology, Charitéplatz 1, 10117 Berlin, Germany

[2]Genomics Core Facility, European Molecular Biology Laboratories, Meyerhofstraße 1, 69117 Heidelberg, Germany

[3]Deutsches Rheumaforschungszentrum, Charitéplatz 1, 10117 Berlin, Germany

[4]Microscopy Core Facility, Max-Planck-Institute for Infection Biology, Charitéplatz 1, 10117 Berlin, Germany

[5]Immune Dynamics and Intravital Microscopy, Charité Universitätsmedizin, Charitéplatz 1, 10117 Berlin, Germany

[6]Wellcome Trust Sanger Institute and European Bioinformatics Institute, Wellcome Genome Campus, Hinxton, Cambridge, CB10 1SD, UK

[7]Lead contact

*Correspondence: levashina@mpiib-berlin.mpg.de

ABSTRACT

Mosquito blood cells are ancestral immune cells that help control infection by vector-borne pathogens. Despite their importance, little is known about mosquito blood cell biology beyond the ambiguous morphological and functional criteria used for their classification. Here we combined the power of single-cell RNA-sequencing, imaging flow cytometry and single-molecule RNA hybridization to analyze blood cells of the malaria mosquito *Anopheles gambiae*. By demonstrating that blood cells express nearly half of the mosquito transcriptome, our dataset represents an unprecedented view into their transcriptional machinery. Analyses of differentially expressed genes identified transcriptional signatures of two distinct cell types that challenge the current morphology-based classification of these cells. We further demonstrated an active transfer of a cellular marker between blood cells that confounds their identity. We propose that cell-to-cell exchange is broadly relevant for cell type classification and may account for the remarkable cellular diversity observed in nature.

INTRODUCTION

The cell is the basic building block of all living organisms. All the major decisions coordinating systems at the organismal level, be it life or death, health or disease, start within a cell. In eukaryotes, multicellularity came with cell compartmentalization and specialization. Cells found in the blood, or hemolymph in invertebrates, have received numerous denominations, such as hemocytes, amebocytes, phagocytes, coelomocytes and immunocytes (Ottaviani and Franceschi, 1997). Regardless of their names, these cells play key roles in shaping the extracellular environment and helping fight infection all throughout the animal kingdom. In insects, blood cells are found circulating by the flow of hemolymph, or as sessile cells associated with internal organs (Ribeiro and Brehelin, 2006). These cells are considered the equivalent of leukocytes in mammals, and display extraordinary functional resemblances to neutrophils, monocytes and macrophages, e.g. phagocytic abilities, chemotaxis, production of antimicrobial peptides, free radicals and cytokine-like molecules (Bergin et al., 2005; Browne et al., 2013; Buchmann, 2014; Costa et al., 2005; Lavine and Strand, 2002). Contrary to the well-established classification of human leukocytes, blood cell type classification is controversial in insects, with

54 similar terms being used for different cell morphologies even within the same insect order
55 (Brayner et al., 2005; Castillo et al., 2006; Hernandez et al., 1999; Ribeiro and Brehelin, 2006).
56 Of note, most studies of insect blood cells have focused on the embryonic and larval stages of
57 the *Drosophila* model (Brandt et al., 2008; Vlisidou and Wood, 2015; Wood and Jacinto, 2007)
58 and these observations are not immediately applicable to other insects (Ribeiro and Brehelin,
59 2006; Zdobnov et al., 2002), particularly in the study of the adult life stages of insects implicated
60 in disease transmission to humans.

61 Mosquitoes are the deadliest animals on Earth, transmitting pathogens that cause a variety of
62 diseases and infect millions of people worldwide every year (WHO, 2014). While feeding on blood
63 to reproduce, adult female mosquitoes acquire blood-borne pathogens from an infected host.
64 Pathogen development and replication within the mosquito is an absolute requirement for further
65 transmission, so the disease cycle is, in part, determined by the mosquitoes' capacity to
66 counterattack these pathogens. Mosquito blood cells are of vital importance in this process as
67 they represent the cellular arm of mosquito immunity, and also participate in humoral responses
68 by secreting pathogen-killing factors, such as components of the melanization pathway (Hillyer et
69 al., 2003; Yassine et al., 2012) and of the complement-like system that help eliminate malaria
70 parasites (Blandin et al., 2004; Frolet et al., 2006). Earlier transcriptomics studies based on
71 microarrays have explored the molecular basis of mosquito hemocyte immunity upon infection
72 with bacteria and *Plasmodium* (Baton et al., 2009; Pinto et al., 2009). More recently, Smith et al
73 used mass spectrometry to analyze mosquito hemocytes isolated based on their uptake of
74 magnetic beads (Smith et al., 2016). To identify genes and proteins more predominantly
75 expressed in hemocytes or in 'phagocytes', these studies relied on enrichment analyses of blood
76 cells relative to whole body or total hemolymph samples, respectively. This restricted the
77 identification of genes co-expressed in blood cells and other tissues, and masked the contribution
78 of sessile hemocytes to overall systemic responses. Such approaches are standard in the study
79 of hemocyte biology, mainly due to the practical constraints associated with the scarcity of these
80 cells and the lack of cellular markers for successful hemocyte isolation and purification.

81 Importantly, the absence of cellular markers has also precluded the classification of mosquito
82 blood cells beyond morphology and function. To date, mosquito hemocytes are morphologically
83 divided based on label-free light microscopy into: (1) granulocytes, phagocytic cells that exhibit
84 granules in their cytoplasm and quickly spread onto glass; (2) oenocytoids, spherical and poorly
85 adhesive cells that produce phenoloxidases involved in melanization defenses; and (3)
86 prohemocytes, small cells of reportedly 2 μm (Rodrigues et al., 2010; Smith et al., 2015) or 4-6

87 μm in size that have been suggested to function as hemocyte progenitors (Castillo et al., 2006),
88 and/or represent small phagocytic cells arising from asymmetrical divisions (King and Hillyer,
89 2013). Although it has been demonstrated that mosquito hemocytes increase in numbers upon
90 blood feeding and infection, in the absence of known hematopoietic organs (Bryant and Michel,
91 2014; King and Hillyer, 2013), the pathways underlining their differentiation into these three
92 classes remain unknown. Whether the current classification represents true discrete cell types or
93 states, and if mosquito blood cell subpopulations exist, are also yet to be explored. In humans
94 and mice, single-cell transcriptomics have recently began to tackle similar questions. It is now
95 also increasingly evident that significant functional differences and considerable variability in gene
96 expression can be recognized in cells long considered to be of the same type (Gaublomme et al.,
97 2015; Grun et al., 2015; Shalek et al., 2014). The use of single-cell approaches to explore cellular
98 heterogeneity in non-model organisms holds the promise to uncover unforeseen complexity, and
99 identify cellular populations that would be forever 'masked' in bulk, enrichment-based
100 measurements. In addition, single-cell studies of invertebrates can contribute to comparative
101 analyses of cellular diversity across different systems.

102 Here we unravel the molecular fingerprint of a subset of mosquito blood cells at a single-cell level,
103 and show that naïve, unstimulated hemocytes express nearly half of the mosquito transcriptome.
104 Our dataset represents a valuable resource for further studies of transcriptional regulation in
105 mosquitoes, and paves the way for the identification of new molecules controlling infection by
106 vector-borne pathogens. By applying fluorescence-activated cell sorting (FACS), single-cell RNA-
107 sequencing (scRNA-seq) and high-content imaging flow cytometry to the analysis of mosquito
108 hemocytes, our unparalleled study identifies two distinct blood cell subpopulations, which we
109 propose to call plasmatocytes and melanocytes. Remarkably, the identified cell subsets do not
110 directly correspond to the current morphological and functional classification of mosquito blood
111 cells, and indicate that the emerging observations of cellular heterogeneity in humans and mice
112 are also characteristic of ancestral blood cells. Our findings further reveal active molecular
113 exchange between mosquito blood cells and the presence of extracellular vesicles (EVs) in the
114 mosquito hemolymph. Shuffling of mRNA and proteins between distinct cell types can influence
115 cellular identity and, in turn, confound cell type identification and classification. Altogether, we
116 demonstrate the power of single-cell technologies in shedding light on the contribution of cell-to-
117 cell exchange to cellular diversity and provide a new perspective on the discussion of the slippery
118 concept of 'cell types'.

119

120

121 **RESULTS**

122 **Single-cell RNA-sequencing of blood cells from *PPO6::RFP* transgenic mosquitoes**

123 In the absence of hemocyte-specific antibodies and dyes, or of transgenic mosquitoes expressing
124 pan-hemocyte markers, we chose to explore a subset of blood cells identified in a transgenic
125 mosquito strain expressing a red fluorescence reporter (tdTomato, abbreviated herein as RFP)
126 under the control of the *prophenoloxidase 6* (*PPO6*) melanization-related gene (*PPO6::RFP*)
127 (Volohonsky et al., 2015). Melanization is a well-established immune response of invertebrates
128 that controls infection against bacteria and parasites (Abraham et al., 2005; Christensen et al.,
129 2005; Hillyer and Strand, 2014; Michel et al., 2005). Several reports suggest that melanization is
130 mediated by a specific cell population called oenocytoids, which represents approximately 10%
131 of the blood cells (Castillo et al., 2006; Hillyer and Strand, 2014), but these cells have not been
132 directly explored. Our focus was on cells obtained in the absence of infection or blood feeding,
133 i.e. during homeostasis because it provides a baseline for analysis of cell-to-cell variation. Using
134 this transgenic strain, we first investigated whether RFP-positive hemocytes were present in the
135 mosquito circulation. For that, we perfused hemolymph onto microscope slides and identified cells
136 displaying RFP fluorescence within the size range predictive of hemocytes (Figure 1A). RFP
137 signal was also observed in hemocytes attached to the inner abdominal wall of dissected adult
138 female mosquitoes, where fat body cells are most prominent (Figure 1B, arrow). As expected, the
139 hemolymph perfusate was, however, heavily contaminated with a mixture of cells and
140 subcellular/tissue debris (Castillo et al., 2006). To purify live RFP-positive cells, we developed a
141 FACS approach based on RFP expression and Hoechst nuclear staining, and validated our
142 purification method by microscopic inspection of sorted cells (Figure 1C-D). Notably, the sorted
143 cell population corresponded to 0.1% of the total events measured (n=100,000) in the perfusate
144 of at least 10 mosquitoes (see Methods). This is in accordance with previous work indicating that
145 only a small subset of adult mosquito hemocytes produce PPOs (Hillyer and Strand, 2014).

146 Next, we FACS-sorted single blood cells and performed scRNA-seq to capture the transcriptome
147 of single PPO-producing blood cells (Figure 1E). Hemocytes were sorted into a 96-well plate and
148 after sample processing and quality assessment (see Methods), we obtained successful cDNA
149 amplification for 56 single-cells in addition to two pools of 30 cells each, from which 28 high quality
150 cDNA libraries were sequenced, representing 26 single hemocytes and the two pooled samples

151 (Figure S1A-D). As a single mosquito can contain as little as 500 blood cells in the circulation
152 (Bryant and Michel, 2014; Hillyer, 2010), we believe the small number of cells analyzed reflects a
153 combination of technical limitations inherent to our approach. First, blood cell isolation is not trivial
154 in mosquitoes, as it requires hemolymph perfusion under micromanipulation followed by cell
155 purification, posing great difficulty in obtaining high numbers of live cells. Second, mosquito blood
156 cells reportedly vary in size from as little as 2 to 20 μm (Brayner et al., 2005; Bryant and Michel,
157 2016; Castillo et al., 2006; Hernandez et al., 1999), and variability in cell size can significantly
158 affect RNA recovery, as small cells contain small amounts of RNA. The adaptation of the scRNA-
159 seq protocol to the study of an invertebrate system, e.g. the choice of lysis buffer and chemistry,
160 may also have influenced our results, especially since different biological cell types show distinct
161 technical quality features in scRNA-seq experiments (Ilicic et al., 2016). A small number of cells
162 has, nevertheless, been used in other scRNA-seq studies (Shalek et al., 2013; Xue et al., 2013)
163 and does not preclude identification of cellular types when an adequate sequencing depth is used.
164 We, therefore, prioritized the deep sequencing of individually curated, very high-quality samples
165 representing a small subset of cells obtained *ex vivo*.

166 Indeed, our sequencing generated on average 4.5 million reads per sample, well-above the
167 minimum of one million reads previously suggested as a requirement for adequate single-cell
168 studies (Wu et al., 2014). Over 70% of the reads were successfully mapped, with exonic reads
169 comprising of more than 40% (Figure S1E-F and Table S1). All samples achieved saturation at
170 around 2 million reads, comparable to previously observed for mammalian cells (Wu et al., 2014).
171 For further analyses, we discarded one cell as it showed gene expression suggestive of a doublet
172 (Figure S1F). Doublets have been reported in the circulation of adult female mosquitoes (King
173 and Hillyer, 2013) and may fall within a size range comparable to larger hemocytes. Around 3,800
174 genes were detected in each pool, whereas single-cells expressed between 450 and 1,400 genes.
175 Similar expression profiles were obtained for pools and single-cells (Figure 1F) with comparable
176 numbers of detected genes only in single-cells or in the pools (1,100 and 1,200 genes,
177 respectively) (Figure 1G). The marker genes used for FACS-sorting (*PPO6* and *tdTomato*) were
178 identified in both single-cells and pools (Table S2), confirming the efficiency of our method.
179 Altogether, our results show that the transcriptome of mosquito hemocytes comprises of over
180 6,000 genes, of which more than half (3,400) had not been identified in earlier studies (Figure
181 S1G) (Baton et al., 2009; Pinto et al., 2009). In addition, our approach revealed sequences for
182 over 80% (n=914) of the proteins reported by an earlier proteomics approach based on magnetic

183 beads isolation of *A. gambiae* phagocytes (Smith et al., 2016) (Figure S1H), corroborating our
184 findings and demonstrating the higher sensitivity of RNA sequencing as compared to proteomics.

185 Mosquito hemocyte biology has been mostly studied in the context of immunity. We, thus,
186 inspected our dataset for previously identified immune genes. Several members of immune
187 pathways were expressed at low levels in some naïve hemocytes, such as the transcription
188 factors *REL1* (AGAP009515) and *REL2* (AGAP006747), *Cactus* (AGAP007938),
189 *IκBβ* (AGAP009166) and *IκBγ* (AGAP005933), and the receptors *PGRP-LC* (AGAP005203) and
190 *PGRP-S1* (AGAP000536) (Table S2). Components of the complement cascade, e.g. *TEP1*
191 (AGAP010815), *APL1C* (AGAP007033), *LRIM1* (AGAP006348) and *HPX2* (AGAP009033), were
192 also detected in some cells, along with the LPS-induced TNFα transcription factor (LITAF)-like 3
193 (AGAP009053) described to control *Plasmodium* survival in the gut (Smith et al., 2015). The
194 phagocytic and antibacterial activities of these cells can be illustrated by the expression of *Eater*
195 (AGAP012386), *Ninjurin* (AGAP006745) and *Nimrod* (AGAP009762), alongside that of several
196 fibrinogen-related proteins (FREPs/FBNs), such as *FBN8* (AGAP011223), *FBN9* (AGAP011197),
197 *FBN10* (AGAP011230) and *FBN30* (AGAP006914) (Dong and Dimopoulos, 2009; Estevez-Lao
198 and Hillyer, 2014; Lombardo et al., 2013). Although no ortholog for a major *Drosophila* hemocyte
199 marker, hemolectin, has been described in the *A. gambiae* genome, mosquito hemocytes
200 expressed both *Pannier* (AGAP002235) and *Serpent* (AGAP002238) GATA factors, as well as
201 *misshapen* (AGAP006340), which are associated with blood cell differentiation, maturation and
202 activation in fruit fly larvae (Braun et al., 1997; Fossett et al., 2003; Minakhina et al., 2011). Genes
203 involved in cell adhesion and polarity, such as *integrin β-1* (AGAP010233), *laminin*
204 (AGAP010548), *Notch1* (AGAP001015) and *Armadillo* (AGAP001043), and components of
205 extracellular matrix like *collagen type IV* (AGAP009200) were also identified. The processed gene
206 expression data for visualization in single cells is accessible at http://data.teichlab.org. Our
207 transcriptional data suggests that in addition to immunity, naïve blood cells are performing tissue
208 maintenance and morphogenesis tasks.

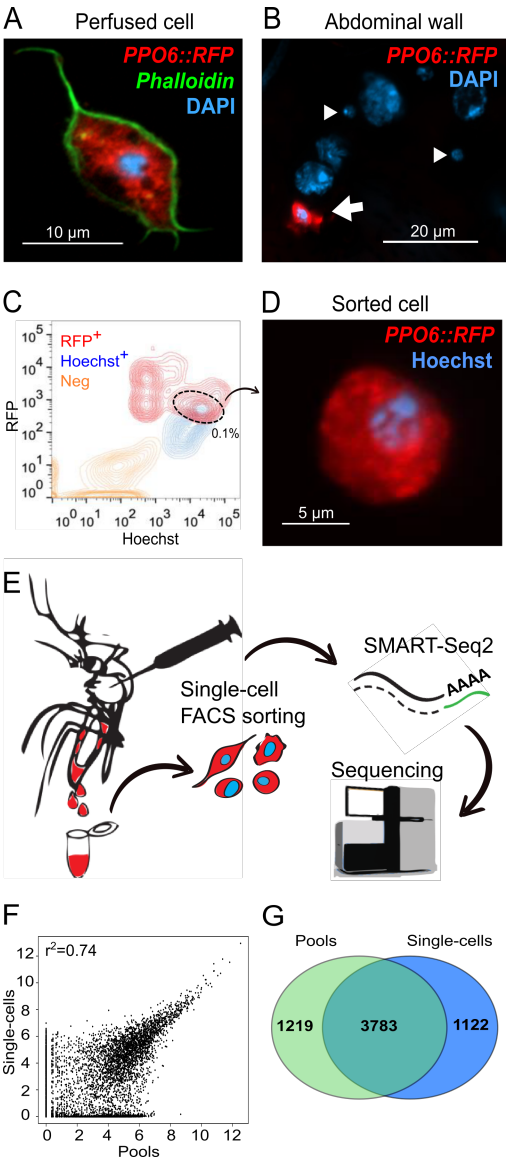

Figure 1: Single-cell RNA-sequencing of transgenic mosquitoes expressing a RFP reporter. A *PPO6::RFP* transgenic mosquito strain was used for isolation of blood cells. (A) A RFP-expressing hemocyte (red) obtained by perfusion of a female adult mosquito. (B) Only a proportion of adult mosquito blood cells display RFP expression (red, arrow), whereas other cells of sizes suggestive of hemocytes do not (arrowhead). (C) FACS sorting of RFP^+ (R^+) $Hoechst^+$ (H^+) blood cells from hemolymph of perfused *PPO6::RFP* mosquito females. (D) Representative image of a sorted cell. (E) The pipeline developed for the study of mosquito blood cells based on single-cell RNA-sequencing. Cells were sorted into a 96-well plate, processed according to the SMART-Seq2 protocol and sequenced in a HiSeq Illumina platform. (F) Scatter plot for the average normalized read counts from pools and single-cells. r^2 indicates Pearson correlation. (G)

220 Venn diagram of genes detected in single-cells and pools (normalized count ≥ 1). Scale bars: (A)
221 10 μm, (B) 20 μm, (D) 5 μm. DNA is stained with DAPI (A-B) and Hoechst (D).

222

223 **Identification of blood cell subpopulations**

224 To account for the technical noise arising from the small amounts of RNA, we included in our
225 samples External RNA Controls Consortium spike-ins (ERCC) prior to cDNA amplification (Baker
226 et al., 2005). We analyzed percentage of spike-ins and mitochondrial counts as a proxy for
227 sequencing efficiency, RNA degradation or incomplete lysis and potential cell death. As
228 anticipated, variation was observed (Figure S1I-J), but caution was taken in applying these criteria
229 and attributing them biological meaning because variability could have arisen from true cell type-
230 related processes. Differences in total number of expressed genes could also have stemmed from
231 different morphologies and cell types. Therefore, we decided not to further discard any cells, and
232 manually curated their individual mappings to confirm that the samples corresponded to
233 potentially true representations of mosquito blood cells. To estimate technical noise, we applied
234 the variability threshold based on the square of the coefficient of variation (CV^2) of the spike-ins
235 (Brennecke et al., 2013), and identified 148 genes whose expression exceeded the variability
236 threshold modeled by the spike-ins (Figure 2A). These highly variable genes included a
237 scavenger receptor, fibrinogen-related and leucine-rich repeat-containing proteins, as well as
238 genes involved in vesicle transport, metabolism and transcription (Table S3). No genes directly
239 associated with cell cycle had high variability, although several *cyclin* genes were detected in
240 specific cells (Table S2), corroborating previous reports of the potential of mosquito hemocytes
241 to undergo cellular division (Bryant and Michel, 2014, 2016; King and Hillyer, 2013).

242 Considering the variable genes, we carried out hierarchical clustering based on pairwise Pearson
243 correlation, which suggested the presence of at least two groups of mosquito blood cells in our
244 samples (Figure 2B). Principal component analysis (PCA) also yielded two cell populations,
245 supporting our clustering results (Figure 2C). Interestingly, the expression levels of *PPO6* showed
246 high variability, and the overlay of *PPO6* expression onto the PCA plot suggested that the two
247 clusters were largely characterized by low and high expression of *PPO6*. Differences in the *PPO6*
248 expression levels have been previously described by immunofluorescence microscopy (Bryant
249 and Michel, 2016) but have not been associated with cell types. Moreover, from the ten *PPO*
250 genes encoded in the *A. gambiae* genome, eight were observed in our sequencing and six of

them, as well as the *RFP* reporter, had variable expression between individual cells and the groups (Figure 2D and Table S3). Hence, we designated these two groups as PPO6^{high} and PPO6^{low}.

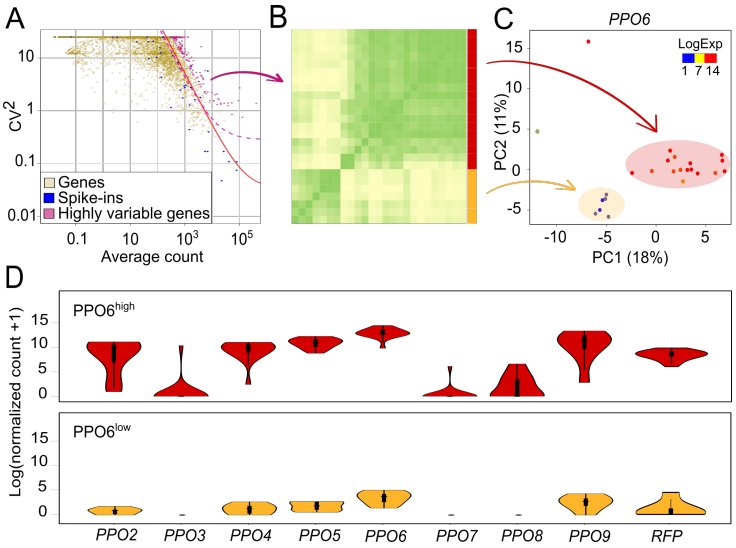

Figure 2: Identification of mosquito blood cell subpopulations. (A) The expression variability of individual genes measured by the squared coefficient of variation (CV^2) is plotted against the mean expression level (normalized counts). Magenta points indicate mosquito genes showing higher than expected expression variability compared with ERCC spike-ins (blue) (adjusted *p* value <0.1). The red line is the fitted line of the spike-ins and the dashed line (pink) marks the margin for genes with 50% biological CV. (B) Pearson correlation heatmap of single hemocytes based on the expression of the highly variable genes identified in (A). Correlation suggests the presence of two groups of cells (red and yellow). (C) PCA plot based on the expression of highly variable genes. The first two principal components are shown, and each point represents one single hemocyte. Two clusters were identified and correspond to the subgroups in (B). *PPO6* expression, as log10 (normalized counts +1), is overlaid onto the PCA plot. (D) Violin plots of *PPOs* and *RFP* expression in the identified groups.

271 **PPO6^{high} and PPO6^{low} cells represent transcriptionally distinct subpopulations**

272 Among the highly variable genes, we detected several *FBN* sequences, such as *FBN8*, *10* and
273 *30*. PPO6^{high} cells showed high expression levels of *FBN10* (Figure 3A, left panel), whereas
274 PPO6^{low} cells exhibited weak or lack expression of *FBN8*, *10* and *30* (Figure 3A, Table S3).
275 Although below the ERCC-defined variability threshold, likely due to the small number of cells
276 analyzed, expression of the antimicrobial peptide gene *lysozyme type I* (*LysI*) (AGAP011119) was
277 more characteristic of PPO6^{low} cells (Figure 3A, middle panel). In the search for a pan-hemocyte
278 marker, we also identified expression of phagocytic receptor *Nimrod* in both groups of cells
279 (Figure 3A, right panel). To validate the *in silico* data, we performed single-molecule RNA
280 fluorescence *in situ* hybridization (RNA-FISH), and observed co-expression of *tdTomato* and
281 *PPO6* in all *PPO6::RFP* hemocytes, with no detection of *tdTomato* in blood cells isolated from
282 wild-type mosquitoes (Figure S2A-B, and data not shown). In terms of *PPO6* levels, RNA-FISH
283 accurately distinguished PPO6^{high} and PPO6^{low} hemocytes, confirming our bioinformatics results.
284 Consistently, PPO6^{high} cells showed high levels of *FBN10*, which were very low or absent in
285 PPO6^{low} cells. High levels of *LysI* were found in PPO6^{low} cells, reinforcing the presence of
286 PPO6^{low}/FBN10^{low}/LysI^{high} cells; and *Nimrod* was near ubiquitously expressed in all perfused
287 hemocytes (Figure 3B). We took advantage of the high conservation levels of *PPO6*, *LysI* and
288 *Nimrod* in the closely related mosquito species, *Anopheles stephensi*, the Asian malaria vector,
289 to explore whether the newly discovered blood cell subgroups were present in other anopheline
290 mosquitoes. Indeed, PPO6^{high} and PPO6^{low}/LysI^{high} cells were seen, along with a low degree of
291 expression of *Nimrod*. No *FBN10* was measured (Figure S2C), probably due to the specificity of
292 the probe to *A. gambiae* and the large diversity of this gene family.

293 To obtain the transcriptional signatures of PPO6^{high} and PPO6^{low} cells, we compared the overall
294 gene expression between these two groups. Based on differentially expressed genes, gene
295 ontology (GO) analyses uncovered that melanization characterized PPO6^{high} cells, whereas
296 metabolism and RNA processing defined the PPO6^{low} subset (Table S4). Although not significant,
297 PPO6^{low} cells appeared to express more genes in total, but mitochondrial counts did not differ
298 between the groups (Figure S2D). These findings suggest that PPO6^{high} cells are specialized for
299 melanization responses, expressing genes involved in these processes at very high levels,
300 whereas PPO6^{low} cells execute a broader range of biological tasks, including melanization. An
301 alternative explanation would be that these groups represent different cell lineages, or perform
302 melanization for diverse processes, e.g. metamorphosis and cuticle sclerotization, as established
303 in other insects (Dudzic et al., 2015; Tsao et al., 2015; Tsao et al., 2009). Transcriptional

304 differences between the two groups could also reflect localization patterns of the cells inside the
305 mosquito body, as blood cells can be found in the circulation or attached to internal organs (King
306 and Hillyer, 2013) and sessile cells could have been displaced during hemolymph perfusion. To
307 assess whether observed differences were related to tissue residency, we performed RNA-FISH
308 in tissues. The analyses of sessile cells revealed both cell populations in close contact with fat
309 body cells within the abdominal wall with no conspicuous cell clusters. The majority of the sessile
310 cells were positive for *Nimrod*, independent of their *PPO* expression (Figure 3C), indicating that
311 *Nimrod* is a potential marker for both circulating and tissue-resident blood cells. Altogether, these
312 results demonstrate that both circulatory and tissue-resident hemocytes display transcriptional
313 heterogeneity, and that $PPO6^{high}$ and $PPO6^{low}$ cell populations are present in two mosquito
314 species.

315

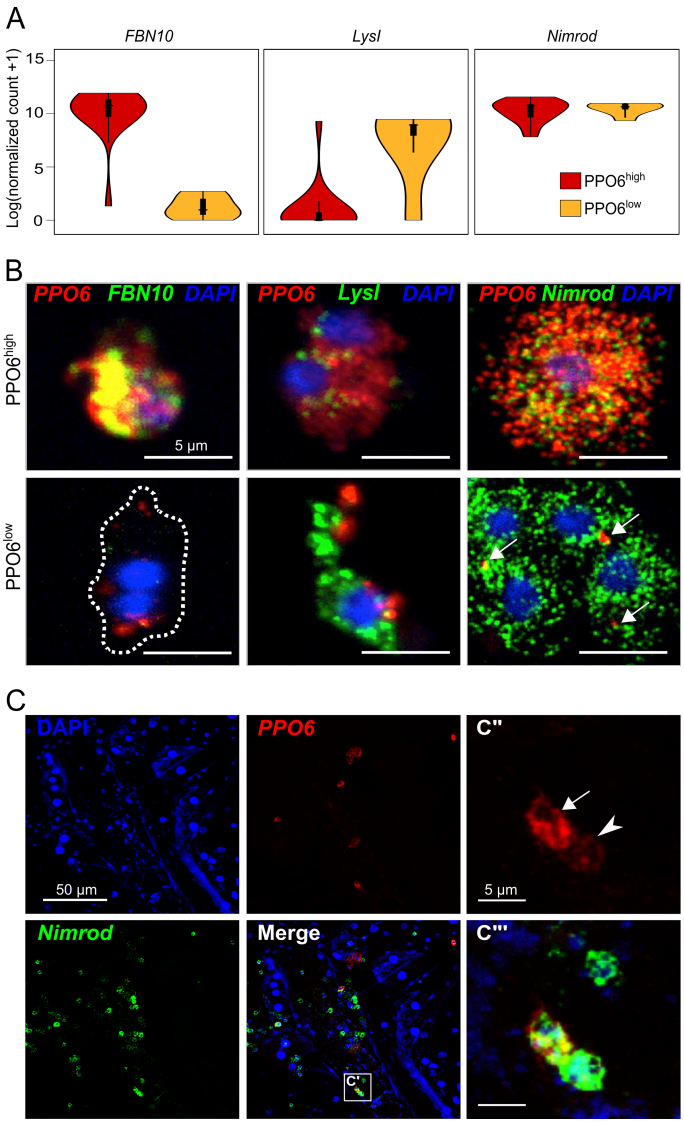

316

317 **Figure 3: Characterization of PPO6^{high} and PPO6^{low} cell subpopulations.** (A) Violin plots of
318 the expression of putative population and pan-hemocyte markers. (B) RNA-FISH validation of
319 identified PPO6^{high} and PPO6^{low} cell subpopulations in perfused cells based on markers shown in
320 (A). Cells were classified as PPO6^{high} (upper panel) or PPO6^{low} (lower panel) according to the
321 expression of *PPO6* (red). Arrows indicate lower *PPO6* signal. (C-C''') PPO6^{high} and PPO6^{low} cell
322 subpopulations can also be seen as tissue-resident blood cells attached to the inner abdominal
323 wall of female mosquitoes. Arrow and arrowhead indicate PPO6^{high} and PPO6^{low} cell
324 subpopulations, respectively. Scale bars: (B) 5 µm, (C) 50 µm, (C''-C''') 5 µm. DNA is stained with
325 DAPI.

326

327 **PPO6^{high} and PPO6^{low} cells share functional and morphological features**

328 Mosquito blood cells are functionally and morphologically separated into three classes -
329 granulocytes, oenocytoids and prohemocytes - based on microscopic studies of surface-attached
330 cells. Our GO analyses suggested the presence of a PPO-specialized cell population and a
331 second cell subset of a less specific nature. Based on that, we reasoned that PPO6^{high} and
332 PPO6^{low} cell groups could be representatives of oenocytoids and granulocytes, respectively. As
333 phagocytosis is a hallmark of granulocytes, we first explored functional differences between these
334 cells using magnetic bead uptake as means for "phagocyte" isolation, as suggested before (Smith
335 et al., 2016). To this end, we injected mosquitoes with magnetic beads and either allowed them
336 to rest at 28°C prior to hemolymph perfusion or incubated the mosquitoes at 4°C to inhibit
337 phagocytosis. To our surprise, both PPO6^{high} and PPO6^{low} cells were identified among
338 magnetically isolated cells and under both conditions, suggesting that instead of phagocytosis,
339 both cell types endocytosed the beads, as no differences in bead uptake were observed when
340 this assay was performed under cold conditions (Figure 4A, arrows). To confirm these findings,
341 we compared the gene profiles of PPO-producing cells to the proteomics results obtained by
342 Smith et al using magnetic bead isolation at 28°C only (Smith et al., 2016). Our analyses revealed
343 that similarities were the strongest when profiles were compared across all samples - PPO6^{high},
344 PPO6^{low}, phagocytes and all cells, i.e. unselected cells obtained in the absence of magnetic
345 isolation. PPO6^{high} and PPO6^{low} shared expression of more genes with phagocytes when
346 considered together rather than alone, indicating that neither PPO6^{high} and PPO6^{low} cell types
347 shared striking similarities with phagocytes at the gene/protein level (Figure 4B). In agreement,
348 nearly all PPOs were present in all samples (Figure 4B'). Overall, these findings did not detect
349 functional differences between PPO6^{high} and PPO6^{low} cells. We conclude that endocytic
350 capabilities likely characterize both granulocytes, considered the "true" phagocytic cell type, and
351 oenocytoids, known as the major source of PPOs.

352 Next, we sought to investigate whether the identified cell populations could be distinguished
353 based on their morphology using imaging flow cytometry and RFP fluorescence as a proxy for
354 *PPO6* expression. We measured a series of morphological features of 319 single RFP-positive
355 cells, which could be divided into RFP^{high} (PPO6^{high}, n=58) and RFP^{low} (PPO6^{low}, n=261) based
356 on their fluorescence intensity (Figures 4C-D and Figure S3). Overall, RFP-positive cells had a
357 mean area of approximately 67 μm^2, ranging from 18 μm^2 to nearly 140 μm^2. These
358 measurements are in accordance with cell sizes reported elsewhere (Bryant and Michel, 2014,
359 2016; Castillo et al., 2006). Similar to recent studies based on flow cytometry of fixed cells (Bryant

360 and Michel, 2014, 2016), we did not detect the cells of 2 μm in size described by other research
361 groups based on label-free light microscopy alone (Rodrigues et al., 2010; Smith et al., 2015).
362 When comparing the cell groups in terms of bright-field measurements of their cytoplasm (see
363 Methods), PPO6^{low} cells showed smaller cytoplasmic area, width, and minor axis than PPO6^{high}
364 cells (Figure 4E and Figure S3). No differences between the groups were detected in granularity
365 or cell shape (Figure S8 and Table S5). To our surprise, PPO6^{high} and PPO6^{low} cells were equally
366 circular. At times, cells from both groups also displayed an elongated shape, typical of the
367 cytoplasmic extensions seen in fusiform or spindle-shaped cells. This fusiform shape is
368 characteristic of plasmatocytes, described in other insects (Ribeiro and Brehelin, 2006). These
369 results failed to morphologically assign RFP-positive cells to any of the morphologically-defined
370 groups: granulocytes, plasmatocytes, or oenocytoids. In fact, the highest discriminating factors
371 (Fisher's linear discriminant, see Methods) separating PPO6^{high} and PPO6^{low} subpopulations
372 relied on RFP intensity alone, with bright-field parameters scoring poorly and failing to establish
373 a morphological distinction between the cells (Table S6). Importantly, our imaging flow cytometry
374 approach relied on morphological analyses of cells in suspension, which is unbiased and likely
375 more relevant for the identification of the cellular types found in the hemolymph circulation. This
376 might explain differences obtained relative to previous studies that focused on cells attached to
377 glass slides, which might be rather reflective of cell 'states' driven by activation of the cellular
378 attachment and adhesion machineries upon exposure to electrostatically charged glass.

379 In addition to RFP intensity, the cell groups differed in their RFP area. PPO6^{high} cells displayed
380 an overall cytoplasmic distribution of the RFP signal, whereas a more localized and globular signal
381 was detected in the cytoplasm of PPO6^{low} cells, where RFP lobes were also more numerous,
382 reinforcing the localized nature of the RFP signal (Figure 4D-E). Microscopic examination also
383 revealed that nearly half of the cells from both groups displayed internal structures and or
384 "budding" extensions of the cytoplasm suggestive of vesicles (Figure 4F-G, arrowhead and arrow,
385 respectively). To confirm that, we performed correlative scanning electron microscopy (SEM) and
386 demonstrated the presence of membrane protrusions or "blebs" in RFP-positive cells (Figure
387 S4A). Altogether, these results established that morphological plasticity of the mosquito blood
388 cells is independent from their transcriptional profile, and that mosquito blood cells have
389 membrane vesicles and protrusions.

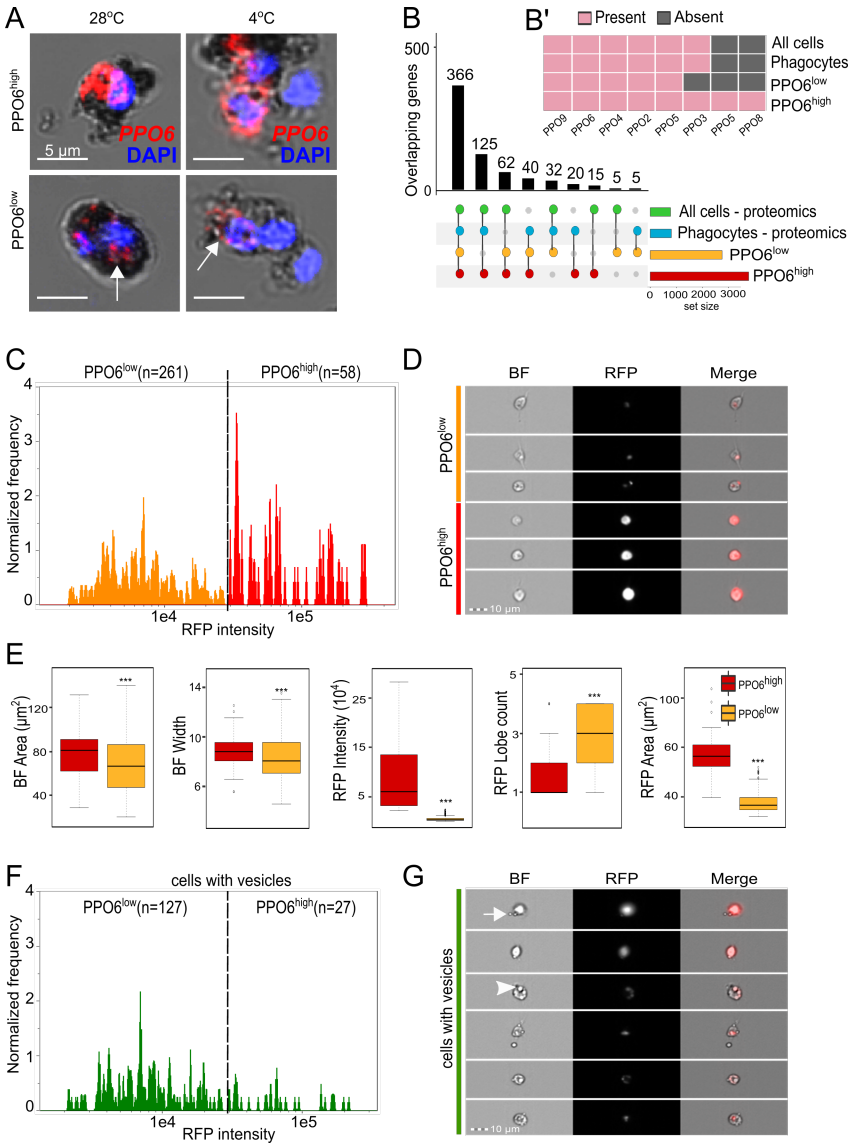

Figure 4: PPO6^{high} and PPO6^{low} cell subpopulations share functional and morphological features. (A) Magnetic bead isolation assays followed by RNA-FISH for identification of cell subpopulations. Arrows indicate lower *PPO6* signal. (B) Intersection analyses between PPO6^{high} and PPO6^{low} cell subpopulations and proteomics results obtained by Smith et al for phagocytes and all cells (unselected). Presence or absence of PPO genes/proteins in each of the samples in shown in (B'). (C) Hemocytes were perfused from *PPO6::RFP* mosquitoes and analyzed using imaging flow cytometry. RFP-positive cells were identified by their RFP Median Pixel and further separated into PPO6^{high} and PPO6^{low} based on their level of RFP fluorescence. The number of cells analyzed per group is shown between parentheses and the dotted line indicates the RFP threshold level used for separation of the two populations. (D) Image gallery containing

401 representative images of PPO6^{high} and PPO6^{low} populations. Variation in cell shape and RFP
402 intensity can be observed in the bright field (BF), RFP and merged images. (E) For every event
403 measured within the flow, a corresponding image and fluorescence levels were acquired and
404 analyzed to generate multiple morphological features. Boxplots show the distribution of five
405 morphological measurements according to the groups. Asterisks represent $p < 0.01$ based on
406 Mann-Whitney-Wilcoxon test. (F) RFP-positive cells were interrogated for the presence of
407 membrane protrusions or internal structures suggestive of vesicles. Similar to (C), cells were
408 grouped into PPO6^{high} and PPO6^{low} and a RFP intensity histogram of cells displaying vesicles
409 (green population) was generated to illustrate that vesicles are observed in cells from both groups.
410 Representative images of cells in this population subset are shown in (G). Arrow and arrowhead
411 indicate representative membrane protrusions and internal vesicles, respectively. See also Figure
412 S4 and Tables S4-5. Boxplots indicate the median, first and third quartile, and min and max
413 values.

414

415 **Mosquito blood cells exchange molecular information**

416 Mosquito hemocytes have been described to produce and secrete EVs (Castillo et al., 2017;
417 Hillyer and Christensen, 2002) and, in agreement, our initial observation suggested that PPO-
418 producing cells display vesicles. We were, therefore, puzzled by the possibility that the RFP signal
419 analyzed in our cell sorting approach could have partially originated from RFP-positive vesicles.
420 Earlier reports used DiD, a lipophilic cyanine dye, to label both mosquito hemocytes and
421 hemocyte-derived vesicles (Castillo et al., 2017; King and Hillyer, 2012). To test whether the
422 localized RFP signal seen in our imaging flow cytometry was associated with vesicles, we first
423 stained PPO-producing cells with DiD and observed that RFP-positive cells indeed contained
424 DiD-positive membrane-bound and internal vesicles that were both RFP-positive and negative
425 (Figure S4B-C). Recently, it has also become clear that EVs are present in extracellular fluids like
426 milk, saliva and plasma, so we reasoned that EVs might be also found in the hemolymph and in
427 association with RFP-negative cells. To identify EVs in the mosquito circulation, we performed
428 imaging flow cytometry analyses using DiD and a recently published approach (Headland et al.,
429 2014). Both DiD-positive cells and EVs could be identified in hemolymph perfusate (Figure 5A-
430 B). EVs were detected based on their small size, weak dark-field and positive DiD fluorescence,
431 with a few EVs also displaying weak RFP signal (Figure 5B, arrowhead). The degree of DiD
432 intensity differed between cells and did not depend on RFP fluorescence. Differential

433 centrifugation followed by electron microscopy confirmed the presence of EVs in hemolymph
434 perfusate of naïve female mosquitoes (Figure 5C). Moreover, SEM of perfused cells also revealed
435 that vesicles of different sizes and shapes, suggestive of the different vesicle types described in
436 the literature - exosomes, microvesicles and apoptotic vesicles (van der Pol et al., 2012), could
437 be indeed observed in association with naïve mosquito blood cells (Figure S4D). These findings
438 suggested that extracellular vesicle production is a general phenomenon that is not limited to
439 PPO-associated cells.

440 A growing body of evidence has demonstrated that RNA can be transferred between mammalian
441 cells. As RNA can be found in EVs, and our data showed that EVs are present in the mosquito
442 hemolymph, we decided to take a step further and explore the possibility that a crosstalk between
443 PPO-positive and negative cells could be responsible for the identification of $PPO6^{high}$ and
444 $PPO6^{low}$ cells. Strengthening this idea were the observations that (1) our scRNA-seq results
445 uncovered cells with minute levels of *PPO6* and *RFP*, and (2) expression of *PPO6* by RNA-FISH
446 was detected inside "budding" extensions associated with PPO6-positive cells (Figure 5D). As a
447 proof of concept, a transwell assay using blood cells from *PPO6::RFP* transgenic and wild-type
448 mosquitoes was developed to test the possibility that RFP mRNA can be transferred between
449 naïve transgenic and wild-type blood cells (Figure 5E). Remarkably, *RFP* transcripts were
450 observed by RNA-FISH inside wild-type blood cells after exposure to hemolymph perfusate from
451 transgenic mosquitoes (Figure 5F, arrowhead). This result indicated that *RFP* mRNAs can be
452 shuttled between blood cells and might account for the $PPO6^{low}$ cell population uncovered by our
453 scRNA-seq and imaging approaches. Taken together, our findings demonstrated that molecular
454 exchange between cells, likely via EVs, can affect their transcriptional profile. As EVs have been
455 shown to carry lipids, proteins and RNA, and can be secreted by virtually all cells, our results
456 revealed an unappreciated role of intercellular molecular exchange in defining cellular identity.

457

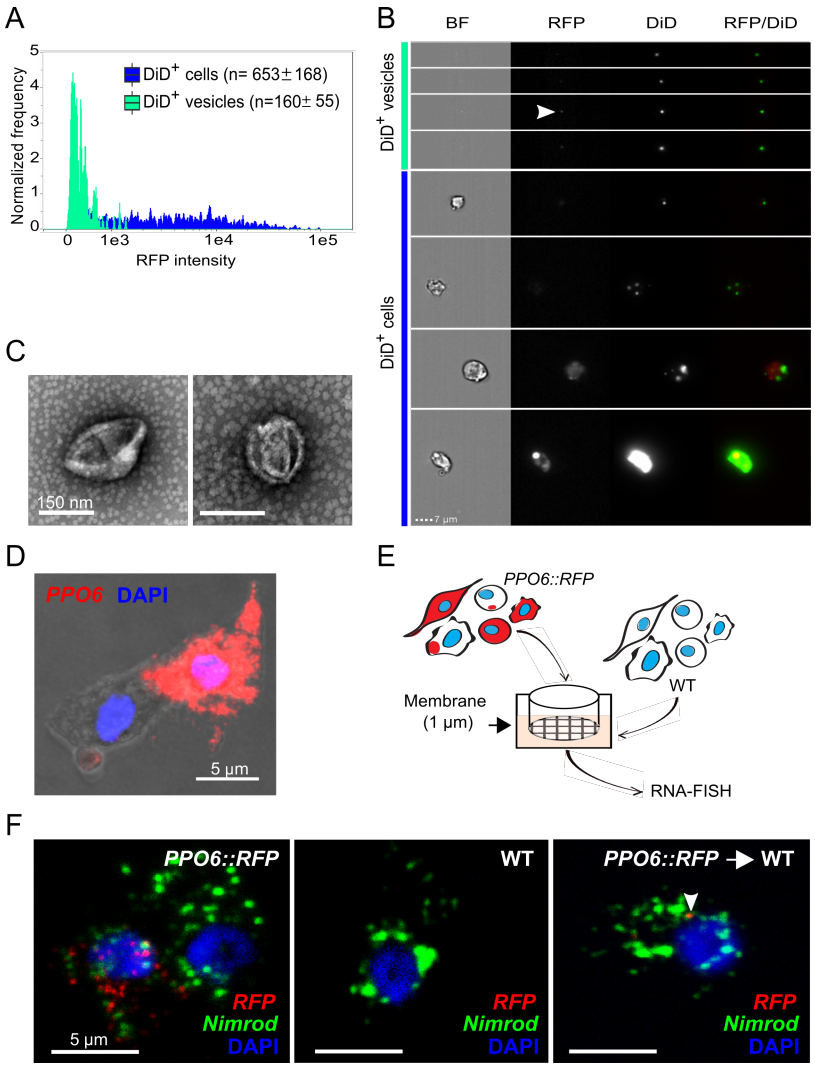

Figure 5: Vesicle identification and molecular exchange in mosquito blood cells. Hemocytes were perfused from *PPO6::RFP* mosquitoes, stained with the lipophilic DiD dye and analyzed using imaging flow cytometry. DiD-positive cells and EVs were first identified according to their DiD and darkfield intensity. EVs were further separated from cells based on their small bright field area. Cells were identified considering their area and aspect ratio. A RFP fluorescence histogram for both DiD-positive cells and EVs in shown in (A). (B) Representative images of DiD-positive cells and EVs. Arrowhead indicates a representative of a RFP-positive vesicle. (C) Negative staining electron microscopy of vesicles obtained by differential centrifugation (10,000xg) of hemolymph perfusate (representative images of 2 independent experiments are shown). (D) *PPO6* mRNA detection by RNA-FISH within budding extensions of blood cells. (E) Schematics of a transwell assay developed to test the transfer of *RFP* between blood cells from *PPO6::RFP* transgenic mosquitoes and wild-type mosquitoes that do not express any reporter

genes. Hemolymph perfusate from wild-type mosquitoes was pipetted onto a coverslip placed under a 1 µm membrane. Perfusate collected from *PPO6::RFP* mosquitoes was placed on top of the membrane. (F) RNA-FISH was performed on coverslips obtained from the transwell assay described in (E) using probes to detect *RFP and Nimrod* expression in wild-type acceptor cells (right panel, arrowhead). Representative images of 2 independent experiments are shown. See also Figure S4.

DISCUSSION

Understanding how transcriptional networks influence cell identity is a central problem in modern molecular biology. Our study describes mosquito blood cells as a source of key components of immunity, development and tissue homeostasis, and places these cells as a central hub coordinating mosquito biology at different levels. Using a combination of single-cell genomics and imaging, we revealed that hemocytes display an unexpected degree of complexity where two transcriptionally defined cellular 'populations' suggestive of distinct cell types share morphological and functional features. We also demonstrate that mosquito blood cells exchange mRNA, leading to the detection, by RNA-FISH, of an "exogenous" gene in acceptor cells. Altogether, our results open a new perspective on cellular crosstalk and cell type classification, in addition to illustrating the power of single-cell-based approaches in discovering unappreciated events at the core of biological processes.

Using single-cell RNA sequencing, we describe the baseline expression of a mosquito blood cell in exceptional detail. An average mosquito blood cell under resting conditions expresses approximately 1,000 genes, or 7% of the mosquito transcriptome. In total, about half of the genes currently annotated in the mosquito genome were detected by RNA sequencing naïve, unstimulated mosquito hemocytes. This represents a substantial gene expression resource for further studies of tissue-specific alternative splicing, RNA editing, gene and transcript models. It will also enable the establishment of transcriptional and regulatory networks that allow for more precise gene enrichment and functional studies. In mosquitoes, where tissue-specific gene knockdown is not available and transgenesis remains limited, functional analyses have greatly relied on the use of dsRNA injections into the open body cavity. This technical limitation restricts the interpretation of tissue-specificity of signaling pathways and their regulation. We believe our dataset will illustrate the importance of tissue specificity studies and pave the road towards the

502 detailed mapping of gene expression in cells and tissues of different systems, with the ultimate
503 goal of creating a comprehensive reference atlas of cellular diversity.

504 By successfully applying single-cell RNA sequencing to the study of blood cells involved in
505 immunity in a major malaria vector, we demonstrated proof of the existence of at least two
506 transcriptionally distinct cell subpopulations that do not represent currently defined cell types. Our
507 results show that the majority of *Anopheles* blood cells likely belong to the PPO6^{low} type. Their
508 rich transcriptional program appears to be reminiscent of granulocytes. The second
509 subpopulation, with a transcriptional profile specialized in melanization, is suggestive of
510 oenocytoids. Nonetheless, these two transcriptionally defined cell types could not be
511 distinguished by the customary functional or morphological tests. Therefore, we propose to call
512 them plasmatocytes and melanocytes. Interestingly, only one cell type, plasmatocytes, is
513 described in the adult *Drosophila* flies. Our transcriptional definition of mosquito blood cells
514 redefines the obscure cellular classification extensively used in studies of hemocytes, and is
515 particularly significant in the context of cellular proliferation and differentiation because mosquito
516 hemocyte lineages are still to be established. Given our results, it will be interesting to address
517 the spatial distribution of mosquito blood cells based on the markers identified here, especially as
518 no lymph glands or hematopoietic cell clusters have been described in mosquitoes. Tissue-
519 resident blood cells likely contribute to local responses and help regulate tissue-specific events.
520 This is exemplified by the recent discovery of macrophage subsets regulating electrical pulsing in
521 the mouse heart (Hulsmans et al., 2017), and of ovarian hemocytes that control collagen IV
522 secretion and germline stem cell niche maintenance in *Drosophila* (Van De Bor et al., 2015).
523 Evidence that cellular heterogeneity can be recognized by profiling single insect blood cells, often
524 called macrophage-like, emphasizes the notion that innate immune cells are far more
525 heterogeneous than previously thought. As macrophages, along with other immune cells, have
526 their evolutionary roots in similar cells in ancestral invertebrates (Buchmann, 2014; Dzik, 2014)
527 and new cell types arise as a result of evolutionary processes (Arendt et al., 2016), the study of
528 insect blood cells can help elucidate the origins of the immune system.

529 In humans and mice, distinct levels and patterns of fluorescence of cellular markers are widely
530 used in microscopy and flow cytometry as a means to cell type classification. Cellular crosstalk
531 may, however, affect such approaches. Acquisition of macrophage-derived “blebs” by
532 lymphocytes has been described, resulting in misrepresentation of lymphocytes as macrophages
533 in flow cytometry studies, and suggesting that these two cells may interact to control early
534 responses in the lymph node (Gray et al., 2012). More importantly, translation of transferred

535 mRNAs into functional proteins has been demonstrated before (Valadi et al., 2007) along with the
536 reprogramming of acceptor cells upon microvesicle-mediated exchange (Ratajczak et al., 2006).
537 It is, therefore, intriguing to consider that expression of specific cellular markers might be
538 influenced by EV uptake. In this scenario, signals sent via vesicles include protein-coding RNAs
539 that are normally absent in acceptor cells, which once translated, appear to be an endogenous
540 cellular marker characteristic of the donor cell population. This observation calls for a critical
541 reassessment of cellular markers by the scientific community. It is also imperative to investigate
542 whether certain protein-coding RNAs are preferentially exchanged compared to other RNAs found
543 in the cells. How *PPO6* and *RFP* transcripts, and potentially other *PPO* genes, contribute to the
544 function of acceptor cells is another exciting question. PPO proteins lack the signal peptides
545 required for their secretion, and it has been suggested that PPO6 is secreted by exocytosis as
546 cell rupture has not been observed (Bryant and Michel, 2016). It is plausible that PPO transcripts
547 are shed by professional melanocytes and processed by non-professional plasmatocytes that
548 locally activate melanization only under specific conditions, e.g. upon infection with specific
549 pathogens, or during wounding and tissue repair. Molecular signals exchanged between cells
550 can, thus, coordinate cellular plasticity and account for the diversity of functional subsets or
551 'hybrid' cells that express markers of different or multiple cell types.

552 The demonstration of mosquito blood-borne EVs indicates that different cells and tissues likely
553 communicate through vesicles secreted into the insect open circulatory system. Several recent
554 reports have suggested EV-mediated immune responses in dipteran insects. Exosome-like
555 vesicles containing virus-derived siRNAs have been identified in *Drosophila* and contribute to
556 systemic antiviral immunity (Tassetto et al., 2017). Apoptotic vesicles released by hemocytes in
557 the proximity of invading parasites have been implicated in anti-*Plasmodium* responses by
558 activating the complement pathway in *A. gambiae* mosquitoes (Castillo et al., 2017). Interestingly,
559 using a GFP reporter strain, Volohonsky et al recently reported that, the anti-malaria mosquito
560 complement-like factor TEP1 is predominately expressed in the fat body as a transcript, but at
561 the protein level it is found in hemocytes upon blood feeding and infection (Volohonsky et al.,
562 2017). The authors speculate this is due to the uptake by the blood cells of TEP1 attached to
563 bacterial cells. As only one plasmatocyte containing low levels of *TEP1* was identified in our
564 sequencing, we suggest that EV-mediated delivery of TEP1 (mRNA or protein) may better explain
565 these surprising findings. We propose that vesicles found in the mosquito hemolymph contain
566 proteins and transcripts that coordinate cell-to-cell and tissue communication not only in infection
567 but also under physiological conditions. Disturbance in homeostasis, be it by infection, metabolic

568 changes, tissue damage or stress, may further escalate secretion of vesicles containing an array
569 of different cargo that can be targeted to specific tissues and complement systemic responses.
570 This represents an outstanding parallel between insects and humans, where EVs found in human
571 body fluids can elicit changes in function and gene expression in target cells, and have a direct
572 role in processes like differentiation, neuronal signaling and cancer. We believe that, similar to
573 how environment, microbiota and genetic make-up influence phenotypic variation, cellular
574 exchange can also drive cellular identity and represents an inventive and unexplored way through
575 which nature coordinates who and what we are.

576

577 **ACKNOWLEDGMENTS**

578 The authors thank Suzana Zakoviz for sharing the drawing in Figure 1, and all members of the
579 Vector Biology Unit for intellectual input and technical support. The authors are grateful to Dr. N.
580 Regev-Rudzki for discussions and critical reading of the manuscript. The authors thank Dr. E.
581 Marois (UPR9022 CNRS, U963 Inserm, France) for sharing the transgenic *PPO6::RFP* line, Dr.
582 K. Müller (Humboldt University, Berlin) for providing *Anopheles stephensi* mosquitoes and
583 acknowledge the discussions in the frame of the CNRS LIA "REL2 and resistance to malaria"
584 project. We also acknowledge the support provided by the Flow Cytometry Core Facility
585 (DRFZ/MPIIB, Berlin) and by Dr. I. Wagner (the Microarrays Core Facility, MPIIB, Berlin).

586

587 **AUTHOR CONTRIBUTIONS**

588 M.S.S. and E.A.L. conceived the study, designed the experiments, analyzed the data and wrote
589 the manuscript. M.S.S. performed all experiments with assistance from R.L.L. for the imaging flow
590 cytometry studies, C.G. and V.B. for the EM analyses, and P.C. for the scRNA-seq. M.S.S. and
591 J.J.M.L. performed bioinformatics analyses. J.H. developed web interface for data interrogation.
592 A.E.H. provided infrastructure. V.B. and S.A.T. provided expert input.

593

594 **DECLARATION OF INTERESTS**

595 The authors declare no competing interests.

596

597 **REFERENCES**

598 Abraham, E.G., Pinto, S.B., Ghosh, A., Vanlandingham, D.L., Budd, A., Higgs, S., Kafatos, F.C.,
599 Jacobs-Lorena, M., and Michel, K. (2005). An immune-responsive serpin, SRPN6, mediates
600 mosquito defense against malaria parasites. Proceedings of the National Academy of Sciences
601 of the United States of America *102*, 16327-16332.

602 Alexa, A., Rahnenfuhrer, J., and Lengauer, T. (2006). Improved scoring of functional groups from
603 gene expression data by decorrelating GO graph structure. Bioinformatics *22*, 1600-1607.

604 Arendt, D., Musser, J.M., Baker, C.V., Bergman, A., Cepko, C., Erwin, D.H., Pavlicev, M.,
605 Schlosser, G., Widder, S., Laubichler, M.D.*, et al.* (2016). The origin and evolution of cell types.
606 Nature reviews Genetics *17*, 744-757.

607 Baker, S.C., Bauer, S.R., Beyer, R.P., Brenton, J.D., Bromley, B., Burrill, J., Causton, H., Conley,
608 M.P., Elespuru, R., Fero, M.*, et al.* (2005). The External RNA Controls Consortium: a progress
609 report. Nat Methods *2*, 731-734.

610 Baton, L.A., Robertson, A., Warr, E., Strand, M.R., and Dimopoulos, G. (2009). Genome-wide
611 transcriptomic profiling of Anopheles gambiae hemocytes reveals pathogen-specific signatures
612 upon bacterial challenge and Plasmodium berghei infection. BMC genomics *10*, 257.

613 Bergin, D., Reeves, E.P., Renwick, J., Wientjes, F.B., and Kavanagh, K. (2005). Superoxide
614 production in Galleria mellonella hemocytes: identification of proteins homologous to the NADPH
615 oxidase complex of human neutrophils. Infection and immunity *73*, 4161-4170.

616 Blandin, S., Shiao, S.H., Moita, L.F., Janse, C.J., Waters, A.P., Kafatos, F.C., and Levashina,
617 E.A. (2004). Complement-like protein TEP1 is a determinant of vectorial capacity in the malaria
618 vector Anopheles gambiae. Cell *116*, 661-670.

619 Brandt, S.M., Jaramillo-Gutierrez, G., Kumar, S., Barillas-Mury, C., and Schneider, D.S. (2008).
620 Use of a Drosophila model to identify genes regulating Plasmodium growth in the mosquito.
621 Genetics *180*, 1671-1678.

622 Braun, A., Lemaitre, B., Lanot, R., Zachary, D., and Meister, M. (1997). Drosophila immunity:
623 analysis of larval hemocytes by P-element-mediated enhancer trap. Genetics *147*, 623-634.

624 Brayner, F.A., Araujo, H.R., Cavalcanti, M.G., Alves, L.C., and Peixoto, C.A. (2005).
625 Ultrastructural characterization of the hemocytes of Culex quinquefasciatus (DIPTERA:
626 Culicidae). Micron *36*, 359-367.

627 Brennecke, P., Anders, S., Kim, J.K., Kolodziejczyk, A.A., Zhang, X., Proserpio, V., Baying, B.,
628 Benes, V., Teichmann, S.A., Marioni, J.C*., et al.* (2013). Accounting for technical noise in single-
629 cell RNA-seq experiments. Nat Methods *10*, 1093-1095.

630 Browne, N., Heelan, M., and Kavanagh, K. (2013). An analysis of the structural and functional
631 similarities of insect hemocytes and mammalian phagocytes. Virulence *4*, 597-603.

632 Bryant, W.B., and Michel, K. (2014). Blood feeding induces hemocyte proliferation and activation
633 in the African malaria mosquito, Anopheles gambiae Giles. The Journal of experimental biology
634 *217*, 1238-1245.

635 Bryant, W.B., and Michel, K. (2016). Anopheles gambiae hemocytes exhibit transient states of
636 activation. Developmental and comparative immunology *55*, 119-129.

637 Buchmann, K. (2014). Evolution of Innate Immunity: Clues from Invertebrates via Fish to
638 Mammals. Frontiers in immunology *5*, 459.

639 Castillo, J.C., Ferreira, A.B.B., Trisnadi, N., and Barillas-Mury, C. (2017). Activation of mosquito
640 complement antiplasmodial response requires cellular immunity. Sci Immunol *2*.

641 Castillo, J.C., Robertson, A.E., and Strand, M.R. (2006). Characterization of hemocytes from the
642 mosquitoes Anopheles gambiae and Aedes aegypti. Insect biochemistry and molecular biology
643 *36*, 891-903.

644 Christensen, B.M., Li, J., Chen, C.C., and Nappi, A.J. (2005). Melanization immune responses in
645 mosquito vectors. Trends in parasitology *21*, 192-199.

646 Costa, S.C., Ribeiro, C., Girard, P.A., Zumbihl, R., and Brehelin, M. (2005). Modes of
647 phagocytosis of Gram-positive and Gram-negative bacteria by Spodoptera littoralis granular
648 haemocytes. J Insect Physiol *51*, 39-46.

649 Dobin, A., Davis, C.A., Schlesinger, F., Drenkow, J., Zaleski, C., Jha, S., Batut, P., Chaisson, M.,
650 and Gingeras, T.R. (2013). STAR: ultrafast universal RNA-seq aligner. Bioinformatics *29*, 15-21.

651 Dong, Y., and Dimopoulos, G. (2009). Anopheles fibrinogen-related proteins provide expanded
652 pattern recognition capacity against bacteria and malaria parasites. The Journal of biological
653 chemistry *284*, 9835-9844.

654 Dudzic, J.P., Kondo, S., Ueda, R., Bergman, C.M., and Lemaitre, B. (2015). Drosophila innate
655 immunity: regional and functional specialization of prophenoloxidases. BMC biology *13*, 81.

656 Dzik, J.M. (2014). Evolutionary roots of arginase expression and regulation. Frontiers in
657 immunology *5*, 544.

658 Estevez-Lao, T.Y., and Hillyer, J.F. (2014). Involvement of the Anopheles gambiae Nimrod gene
659 family in mosquito immune responses. Insect biochemistry and molecular biology *44*, 12-22.

660 Fossett, N., Hyman, K., Gajewski, K., Orkin, S.H., and Schulz, R.A. (2003). Combinatorial
661 interactions of serpent, lozenge, and U-shaped regulate crystal cell lineage commitment during
662 Drosophila hematopoiesis. Proceedings of the National Academy of Sciences of the United States
663 of America *100*, 11451-11456.

664 Frolet, C., Thoma, M., Blandin, S., Hoffmann, J.A., and Levashina, E.A. (2006). Boosting NF-
665 kappaB-dependent basal immunity of Anopheles gambiae aborts development of Plasmodium
666 berghei. Immunity *25*, 677-685.

667 Gaublomme, J.T., Yosef, N., Lee, Y., Gertner, R.S., Yang, L.V., Wu, C., Pandolfi, P.P., Mak, T.,
668 Satija, R., Shalek, A.K.*, et al.* (2015). Single-Cell Genomics Unveils Critical Regulators of Th17
669 Cell Pathogenicity. Cell *163*, 1400-1412.

670 Gray, E.E., Friend, S., Suzuki, K., Phan, T.G., and Cyster, J.G. (2012). Subcapsular sinus
671 macrophage fragmentation and CD169+ bleb acquisition by closely associated IL-17-committed
672 innate-like lymphocytes. PloS one *7*, e38258.

673 Grun, D., Lyubimova, A., Kester, L., Wiebrands, K., Basak, O., Sasaki, N., Clevers, H., and van
674 Oudenaarden, A. (2015). Single-cell messenger RNA sequencing reveals rare intestinal cell
675 types. Nature *525*, 251-255.

676 Headland, S.E., Jones, H.R., D'Sa, A.S., Perretti, M., and Norling, L.V. (2014). Cutting-edge
677 analysis of extracellular microparticles using ImageStream(X) imaging flow cytometry. Sci Rep *4*,
678 5237.

679 Hernandez, S., Lanz, H., Rodriguez, M.H., Torres, J.A., Martinez-Palomo, A., and Tsutsumi, V.
680 (1999). Morphological and cytochemical characterization of female Anopheles albimanus
681 (Diptera: Culicidae) hemocytes. Journal of medical entomology *36*, 426-434.

682 Hillyer, J.F. (2010). Mosquito immunity. Advances in experimental medicine and biology *708*, 218-
683 238.

684 Hillyer, J.F., and Christensen, B.M. (2002). Characterization of hemocytes from the yellow fever
685 mosquito, Aedes aegypti. Histochemistry and cell biology *117*, 431-440.

686 Hillyer, J.F., Schmidt, S.L., and Christensen, B.M. (2003). Rapid phagocytosis and melanization
687 of bacteria and Plasmodium sporozoites by hemocytes of the mosquito Aedes aegypti. The
688 Journal of parasitology *89*, 62-69.

689 Hillyer, J.F., and Strand, M.R. (2014). Mosquito hemocyte-mediated immune responses. Current
690 Opinion in Insect Science.

691 Hulsmans, M., Clauss, S., Xiao, L., Aguirre, A.D., King, K.R., Hanley, A., Hucker, W.J., Wulfers,
692 E.M., Seemann, G., Courties, G.*, et al.* (2017). Macrophages Facilitate Electrical Conduction in
693 the Heart. Cell *169*, 510-522 e520.

694 Ilicic, T., Kim, J.K., Kolodziejczyk, A.A., Bagger, F.O., McCarthy, D.J., Marioni, J.C., and
695 Teichmann, S.A. (2016). Classification of low quality cells from single-cell RNA-seq data. Genome
696 Biol *17*, 29.

697 King, J.G., and Hillyer, J.F. (2012). Infection-induced interaction between the mosquito circulatory
698 and immune systems. PLoS pathogens *8*, e1003058.

699 King, J.G., and Hillyer, J.F. (2013). Spatial and temporal in vivo analysis of circulating and sessile
700 immune cells in mosquitoes: hemocyte mitosis following infection. BMC biology *11*, 55.

701 Kowal, J., Arras, G., Colombo, M., Jouve, M., Morath, J.P., Primdal-Bengtson, B., Dingli, F., Loew,
702 D., Tkach, M., and Thery, C. (2016). Proteomic comparison defines novel markers to characterize

703 heterogeneous populations of extracellular vesicle subtypes. Proceedings of the National
704 Academy of Sciences of the United States of America *113*, E968-977.

705 Lavine, M.D., and Strand, M.R. (2002). Insect hemocytes and their role in immunity. Insect
706 biochemistry and molecular biology *32*, 1295-1309.

707 Lawson, D., Arensburger, P., Atkinson, P., Besansky, N.J., Bruggner, R.V., Butler, R., Campbell,
708 K.S., Christophides, G.K., Christley, S., Dialynas, E.*, et al.* (2007). VectorBase: a home for
709 invertebrate vectors of human pathogens. Nucleic Acids Res *35*, D503-505.

710 Lombardo, F., Ghani, Y., Kafatos, F.C., and Christophides, G.K. (2013). Comprehensive genetic
711 dissection of the hemocyte immune response in the malaria mosquito Anopheles gambiae. PLoS
712 pathogens *9*, e1003145.

713 Love, M.I., Huber, W., and Anders, S. (2014). Moderated estimation of fold change and dispersion
714 for RNA-seq data with DESeq2. Genome Biol *15*, 550.

715 Michel, K., Budd, A., Pinto, S., Gibson, T.J., and Kafatos, F.C. (2005). Anopheles gambiae
716 SRPN2 facilitates midgut invasion by the malaria parasite Plasmodium berghei. EMBO reports *6*,
717 891-897.

718 Minakhina, S., Tan, W., and Steward, R. (2011). JAK/STAT and the GATA factor Pannier control
719 hemocyte maturation and differentiation in Drosophila. Developmental biology *352*, 308-316.

720 Ottaviani, E., and Franceschi, C. (1997). The invertebrate phagocytic immunocyte: clues to a
721 common evolution of immune and neuroendocrine systems. Immunology today *18*, 169-174.

722 Picelli, S., Bjorklund, A.K., Faridani, O.R., Sagasser, S., Winberg, G., and Sandberg, R. (2013).
723 Smart-seq2 for sensitive full-length transcriptome profiling in single cells. Nat Methods *10*, 1096-
724 1098.

725 Pinto, S.B., Lombardo, F., Koutsos, A.C., Waterhouse, R.M., McKay, K., An, C., Ramakrishnan,
726 C., Kafatos, F.C., and Michel, K. (2009). Discovery of Plasmodium modulators by genome-wide
727 analysis of circulating hemocytes in Anopheles gambiae. Proceedings of the National Academy
728 of Sciences of the United States of America *106*, 21270-21275.

729 Ratajczak, J., Miekus, K., Kucia, M., Zhang, J., Reca, R., Dvorak, P., and Ratajczak, M.Z. (2006).
730 Embryonic stem cell-derived microvesicles reprogram hematopoietic progenitors: evidence for
731 horizontal transfer of mRNA and protein delivery. Leukemia *20*, 847-856.

732 Ribeiro, C., and Brehelin, M. (2006). Insect haemocytes: what type of cell is that? J Insect Physiol
733 *52*, 417-429.

734 Rodrigues, J., Brayner, F.A., Alves, L.C., Dixit, R., and Barillas-Mury, C. (2010). Hemocyte
735 differentiation mediates innate immune memory in Anopheles gambiae mosquitoes. Science *329*,
736 1353-1355.

737 Shalek, A.K., Satija, R., Adiconis, X., Gertner, R.S., Gaublomme, J.T., Raychowdhury, R.,
738 Schwartz, S., Yosef, N., Malboeuf, C., Lu, D.*, et al.* (2013). Single-cell transcriptomics reveals
739 bimodality in expression and splicing in immune cells. Nature *498*, 236-240.

740 Shalek, A.K., Satija, R., Shuga, J., Trombetta, J.J., Gennert, D., Lu, D., Chen, P., Gertner, R.S.,
741 Gaublomme, J.T., Yosef, N.*, et al.* (2014). Single-cell RNA-seq reveals dynamic paracrine control
742 of cellular variation. Nature *510*, 363-369.

743 Smith, R.C., Barillas-Mury, C., and Jacobs-Lorena, M. (2015). Hemocyte differentiation mediates
744 the mosquito late-phase immune response against Plasmodium in Anopheles gambiae.
745 Proceedings of the National Academy of Sciences of the United States of America *112*, E3412-
746 3420.

747 Smith, R.C., King, J.G., Tao, D., Zeleznik, O.A., Brando, C., Thallinger, G.G., and Dinglasan, R.R.
748 (2016). Molecular profiling of phagocytic immune cells in Anopheles gambiae reveals integral
749 roles for hemocytes in mosquito innate immunity. Mol Cell Proteomics.

750 Tassetto, M., Kunitomi, M., and Andino, R. (2017). Circulating Immune Cells Mediate a Systemic
751 RNAi-Based Adaptive Antiviral Response in Drosophila. Cell *169*, 314-325 e313.

752 Tsao, I.Y., Chen, J.W., Li, C.J., Lo, H.L., Christensen, B.M., and Chen, C.C. (2015). The dual
753 roles of Armigeres subalbatus prophenoloxidase V in parasite melanization and egg chorion
754 melanization in the mosquito Ar. subalbatus. Insect biochemistry and molecular biology *64*, 68-
755 77.

756 Tsao, I.Y., Lin, U.S., Christensen, B.M., and Chen, C.C. (2009). Armigeres subalbatus
757 prophenoloxidase III: Cloning, characterization and potential role in morphogenesis. Insect
758 biochemistry and molecular biology *39*, 96-104.

759 Valadi, H., Ekstrom, K., Bossios, A., Sjostrand, M., Lee, J.J., and Lotvall, J.O. (2007). Exosome-
760 mediated transfer of mRNAs and microRNAs is a novel mechanism of genetic exchange between
761 cells. Nat Cell Biol *9*, 654-659.

762 Van De Bor, V., Zimniak, G., Papone, L., Cerezo, D., Malbouyres, M., Juan, T., Ruggiero, F., and
763 Noselli, S. (2015). Companion Blood Cells Control Ovarian Stem Cell Niche Microenvironment
764 and Homeostasis. Cell reports *13*, 546-560.

765 van der Pol, E., Boing, A.N., Harrison, P., Sturk, A., and Nieuwland, R. (2012). Classification,
766 functions, and clinical relevance of extracellular vesicles. Pharmacol Rev *64*, 676-705.

767 Vlisidou, I., and Wood, W. (2015). Drosophila blood cells and their role in immune responses.
768 FEBS J *282*, 1368-1382.

769 Volohonsky, G., Hopp, A.K., Saenger, M., Soichot, J., Scholze, H., Boch, J., Blandin, S.A., and
770 Marois, E. (2017). Transgenic Expression of the Anti-parasitic Factor TEP1 in the Malaria
771 Mosquito Anopheles gambiae. PLoS pathogens *13*, e1006113.

772 Volohonsky, G., Terenzi, O., Soichot, J., Naujoks, D.A., Nolan, T., Windbichler, N., Kapps, D.,
773 Smidler, A.L., Vittu, A., Costa, G.*, et al.* (2015). Tools for Anopheles gambiae Transgenesis. G3
774 (Bethesda) *5*, 1151-1163.

775 WHO (2014). A global brief on vector-borne diseases, W.H. Organization, ed. (Geneva,
776 Switzerland: WHO Press).

777 Wood, W., and Jacinto, A. (2007). Drosophila melanogaster embryonic haemocytes: masters of
778 multitasking. Nat Rev Mol Cell Biol *8*, 542-551.

779 Wu, A.R., Neff, N.F., Kalisky, T., Dalerba, P., Treutlein, B., Rothenberg, M.E., Mburu, F.M.,
780 Mantalas, G.L., Sim, S., Clarke, M.F.*, et al.* (2014). Quantitative assessment of single-cell RNA-
781 sequencing methods. Nat Methods *11*, 41-46.

782 Xue, Z., Huang, K., Cai, C., Cai, L., Jiang, C.Y., Feng, Y., Liu, Z., Zeng, Q., Cheng, L., Sun, Y.E.,
783 *et al.* (2013). Genetic programs in human and mouse early embryos revealed by single-cell RNA
784 sequencing. Nature *500*, 593-597.

785 Yassine, H., Kamareddine, L., and Osta, M.A. (2012). The mosquito melanization response is
786 implicated in defense against the entomopathogenic fungus Beauveria bassiana. PLoS
787 pathogens *8*, e1003029.

788 Zdobnov, E.M., von Mering, C., Letunic, I., Torrents, D., Suyama, M., Copley, R.R., Christophides,
789 G.K., Thomasova, D., Holt, R.A., Subramanian, G.M., *et al.* (2002). Comparative genome and
790 proteome analysis of Anopheles gambiae and Drosophila melanogaster. Science *298*, 149-159.

791

792

793 **MATERIALS and METHODS**

794 **Mosquito rearing, fluorescence microscopy and hemolymph perfusion**

795 *Anopheles gambiae sensu lato PPO6::RFP* transgenic (Volohonsky et al., 2015) and wild type
796 strains were reared at 28°C, under 80% humidity and at a 12/12 h day/night cycle. Larvae were
797 fed with cat food and adult mosquitoes were fed *ad libitum* with 10% sugar solution. For tissue
798 microscopy, adult female mosquitoes were dissected in 1 X PBS, fixed in 4% paraformaldehyde
799 (PFA), washed three times and mounted using Vectashield mounting medium containing DAPI.
800 For hemolymph perfusion, 3-5-day-old female mosquitoes were anesthetized on ice for 10 min,
801 microinjected with 700 nl of a buffer containing 60% Schneider's Medium, 10% fetal bovine serum
802 (FBS), and 30% citrate buffer (anticoagulant; 98 mM NaOH, 186 mM NaCl, 1.7 mM EDTA, 41
803 mM citric acid, pH 4.5) and allowed to rest, on ice, for 10 min. A small cut was made between the
804 last two abdominal segments with the help of dissection scissors and the flow through was
805 collected after further injection of 10 µl of buffer. For microscopy analyses, mosquitoes were
806 perfused directly onto glass slides or coverslips, and cells were allowed to attach for at least 15
807 min prior to fixation in 4% PFA. Cells were next stained with a 1:100 dilution of Alexa 488
808 Phalloidin (ThermoFisher) for 30 min at room temperature. For the DiD analyses, cells were
809 stained with DiD (5 µM) for 20 min prior to PFA fixation. Following washes, cells were mounted
810 as described above, and analyzed on a Zeiss Axiovert microscope.

811

812 **FACS and single-cell RNA-sequencing by SMART-Seq2**

813 For FACS and imaging flow cytometry analyses, 10-12 mosquitoes were perfused. Hemolymph
814 perfusate was collected with the help of a pipette, transferred into a siliconized microtube and
815 diluted to a final volume of 500 µl buffer containing 2 µg/ml of Hoechst 3342 (Molecular Probes).
816 Cells were immediately analyzed in a BD ARIA II Cell Sorter equipped with violet and green-
817 yellow lasers at 405 and 561 nm, respectively. Cells were first gated based on their RFP
818 fluorescence, followed by positive Hoechst signal, with Area versus Width measurements being
819 used for doublet discrimination. The FACS machine was standardized with fluorochrome-
820 containing beads and sorting purity was validated by visualization of cells sorted onto a glass
821 coverslip. Cells were sorted into a 96-well PCR plate containing 5 µl of 0.2% Triton X-100
822 supplemented with 2 U/µl of RNAse inhibitor (Clontech), with two wells containing 30 cells each
823 (pool samples) and one column (8 wells) containing only the lysis buffer used as a negative
824 control. We added ERCC spike-ins (Ambion) at a 1:2 billion dilution into the plate prior to cDNA
825 synthesis and all samples were next processed according to the SMART-Seq2 protocol using up
826 to 22 PCR cycles for cDNA synthesis (Picelli et al., 2013). PCR products were purified with
827 AMPure XP beads (Beckman Coulter). Quality control was performed for each sample individually
828 both as cDNA input and sequencing library using a high sensitivity DNA kit (Agilent). A total of
829 125 pg of cDNA was used for library construction. cDNA libraries were pooled at a 10nM final
830 concentration and 100 bp paired end sequencing was performed in one lane using a HiSeq2000
831 Sequencer (Illumina).

832

833 **RNA-seq data analysis**

834 Reads generated by sequencing were demultiplexed using bcl2fastq (version 1.8.4) and mapped
835 to *A. gambiae* genome (P4), ERCC92 (Ambion) and *dTomato* sequence (Volohonsky et al., 2015)
836 with the STAR aligner (version 2.4.2a) (Dobin et al., 2013). The genome index was generated
837 with *A. gambiae* geneset file in gtf format (P4.4) and gene count tables were produced during the
838 mapping (--quantMode Genecounts). They were next normalized with size factors calculated from
839 the ERCCs using DESeq2 (Love et al., 2014). For the purpose of comparisons, a gene was
840 considered expressed if at least one normalized read was identified in at least one sample. Genes

841 were annotated using Vectorbase (Lawson et al., 2007) and manual curation. For comparisons
842 with previous studies (Baton et al., 2009; Pinto et al., 2009; Smith et al., 2016), gene IDs were
843 converted using Vectorbase and BioMart. Intersection analyses were performed in R using the
844 VennDiagram and upsetR packages. Technical noise estimation and identification of the highly
845 variable genes were performed as reported before (Brennecke et al., 2013), using the 60-
846 percentile as the mean cut-off to include more ERCC genes in the technical fit. Principal
847 component analyses were done with the *prcomp* function and differential expression analyses
848 were based on the DESeq2 package, using the ERCC size factors and $PPO6^{low}$ versus $PPO6^{high}$
849 as comparison. For GO analyzes, we used topGO (Alexa et al., 2006) and GO terms were
850 obtained from the org.Ag.eg.db annotation package. Analyses were performed in R and scripts
851 are available upon request. The sequencing results were deposited in the European Nucleotide
852 Archive under the following accession number: PRJEB23372 and the processed expression data
853 can be accessed at http://data.teichlab.org for single gene visualization.

854

855 **Imaging flow cytometry**

856 Ten to twelve sugar-fed *PPO6::RFP* female mosquitoes were perfused to a final volume of 20-40
857 µl and the diluted hemolymph samples were immediately analyzed in an Amnis ImageStreamX
858 MKII (Merck). For *PPO6::RFP* analyses, wild type mosquitoes were used to set background
859 fluorescence and cells were measured with a 40x objective. Comparisons between cell
860 subpopulations were performed using the "Object" mask and based on a built-in function that uses
861 Fisher's discriminant ratio (Rd) to determine the best statistical separation (largest Rd) between
862 identified populations. For the DiD analyses, cells were collected into FBS-free buffer containing
863 1 µM of DiD and analyzed at 60x to increase resolution. Single staining controls representing
864 RFP, DiD and medium alone were used for calibration and manual compensation. Experiments
865 were repeated at least twice. Cell gating was confirmed considering the obtained images and
866 manually curated to exclude debris and doublets that could not be excluded by the gating alone.
867 Vesicle detection was performed as reported before (Headland et al., 2014). Briefly, DiD positive
868 events were interrogated based on their level of DiD fluorescence and size scatter intensity. DiD-
869 labelled vesicles showed a low scatter along with low to mid DiD fluorescence, whereas cells
870 displayed mid to high fluorescence and scatter measurements. Speed beads, used for the
871 instrument calibration and focusing, were easily gated out as a discrete population displaying very
872 high levels of side-scatter intensity. The RFP intensity was measured based on the median pixel

873 by means of histogram, and cellular debris and doublets were excluded according to their
874 brightfield area and aspect ratio. The identified populations were compared using the "Feature
875 Finder" function of the IDEAS software (MilliporeSigma). Statistical analyses were based on
876 Mann-Whitney-Wilcoxon and graphs were done in R.

877

878 **RNA *in situ* hybridization using RNAscope**

879 RNA *in situ* studies were performed according to the RNAscope Multiplex Fluorescence analyses
880 manual (Advanced Cell Diagnostics). Briefly, cells were perfused onto glass slides, allowed to
881 attach and fixed in PFA as described above. If needed, slides were dehydrated and kept in 100%
882 ethanol at -20˚C until processing. Samples from *A. stephensi* were handled following the same
883 procedure. Tissue samples were processed immediately after dissection in RNAse-free PBS. All
884 RNAscope probes were designed by Advanced Cell Diagnostics and are commercially available.
885 Each probe was individually tested against a negative control prior and during each analysis.
886 Images were acquired using a Leica SP8 confocal microscope equipped with 405, 488, 561 and
887 647 nm lasers and prepared for submission using the basic features of the LAS X software.

888

889 **Bead uptake assay**

890 For magnetic isolation of hemocytes, we followed the protocol by Smith et al 2016 with small
891 modifications. Briefly, 20 female mosquitoes were cold anesthetized and injected with 300 µl of a
892 2 mg/ml suspension of MagnaBind Carboxyl Derivatized Beads (Thermo Scientific). Mosquitoes
893 were next kept at 28°C or 4°C for 2 h and perfused as described above. Hemolymph perfused
894 was collected with the help of a pipette tip and transferred into a 0.5 µl Eppendorf tube containing
895 100 ul of injection buffer. Samples were diluted to 200 µl and incubated in a magnetic stand for
896 20 min at 4°C. Supernatant was removed by pipetting, magnetic pellet was resuspended in 1 X
897 RNAse-free PBS and transferred to a microscopy slide. Cells were allowed to attach for 15 min
898 and processed for RNA-FISH as described above.

899

900 **Transwell assay**

901 For this assay, we used *PPO6::RFP* transgenic mosquitoes and the *A. gambiae* Ngousso
902 (TEP1*S1) wild-type mosquito strain. Perfusion was performed in the absence of FBS and
903 hemolymph was collected with the help of a pipette onto the top of a glass coverslip placed inside
904 a 24-well plate. A total of 100 µl of buffer was further gently pipetted onto the cell drop to prevent
905 dehydration. Cell inserts (Merck) were then placed over individual wells and hemolymph perfusate
906 from *PPO6::RFP* female mosquitoes was gently pipetted onto the 1 µm membrane mesh. Diluted
907 hemolymph from at least 2 wild type and 4 transgenic mosquitoes were used per treatment, and
908 the negative control consisted of overlaying coverslips with buffer only. Plates were kept at room
909 temperature for at least 1 h; following by fixation of coverslips with 4% PFA and PBS washes prior
910 to immediate processing based on the RNAscope manual. Images were obtained by confocal
911 microscopy as described above. Experiments were repeated at least twice.

912

913 **Scanning electron microscopy:**

914 For scanning electron microscopy (SEM), cells were perfused from at least 2 female mosquitoes
915 directly onto glass coverslips and fixed with 4% PFA. To facilitate exosome imaging, poly-L-lysine
916 treated coverslips were used. For correlative SEM, cells were placed onto microscopic dishes
917 with finder grids (ibidi) and imaged directly after 4% PFA fixation using a Zeiss Axiovert
918 microscope, prior to SEM processing. The samples were post-fixed in 2.5% glutaraldehyde, 0.5%
919 osmium-tetroxide, tannic acid and osmium-tetroxide again. The coverslips or optical membranes
920 were then dehydrated in a graded ethanol series, dried in carbon dioxide at critical point and
921 vacuum coated with 3 nm Carbon-Platinum. Imaging was performed using a LEO 1550 (Zeiss,
922 Oberkochen DE) scanning-electron microscope. Experiments were repeated at least twice.

923

924 **Transmission electron microscopy:**

925 EVs were isolated according to a protocol described before (Kowal et al., 2016). In summary,
926 hemolymph perfusate from at least 20 mosquitoes was subjected to differential centrifugation at
927 4˚C and the 10,000 x g pellet was processed for negative staining electron microscopy. Aliquots
928 of the samples were applied to freshly glow discharged carbon- and pioloform-film-coated copper
929 grids and allowed to adsorb for 10 min. After washes with distilled water, the grids were contrasted
930 with 2% uranyl acetate, touched on filter paper and air-dried. The grids were examined in a LEO

906 (Zeiss AG, Oberkochen) electron microscope operated at 100 kV and images were recorded with a Morada (SIS-Olympus, Münster) digital camera.